Mechanical and laser impact effects on woven composites with hemp or glass fibres

Fabienne Touchard, Michel Boustié, Laurence Chocinski-Arnault, Pedro Pascual González, Laurent Berthe, Davi Silva de Vasconcellos, Luigi Sorrentino, Pawel H Malinowski, Wieslaw M Ostachowicz

Mechanical and laser impact effects on woven composites with hemp or glass fibres

Fabienne Touchard[a*], Michel Boustie[a], Laurence Chocinski-Arnault[a], Pedro Pascual Gonzalez[a], Laurent Berthe[b], Davi Silva de Vasconcellos[c], Luigi Sorrentino[c], Paweł H. Malinowski[d], Wiesław M. Ostachowicz[d,e]

[a]Institut PPRIME, CNRS, ISAE-ENSMA, Université de Poitiers, 86961 Futuroscope-Chasseneuil, France

[b]PIMM, CNRS-ENSAM Paristech, 151 Bd de l'Hopital, 75013 Paris Cedex, France

[c] Institute for Polymers, Composites and Biomaterials (IPCB)-CNR, Piazzale Enrico Fermi 1, Località Granatello, 80055 Portici (NA), Italy

[d]Institute of Fluid-Flow Machinery, Polish Academy of Sciences, 14 Fiszera St., 80–231 Gdansk, Poland

[e]Faculty of Automotive and Construction Machinery, Warsaw University of Technology, Warsaw, Poland

Abstract

Purpose - The aim of this paper is to study the damage induced in 'green' and synthetic composites under impact loading.

Design/methodology/approach - The study was focused on epoxy based composites reinforced with woven hemp or glass fibres. Six assessment techniques were employed in order to analyse and compare impact damages: eye observation, back face relief, terahertz spectroscopy, laser vibrometry, X-ray micro-tomography and microscopic observations.

Findings - Different damage detection thresholds for each material and technique were obtained. Damage induced by mechanical and laser impacts showed relevant differences but the damage mechanisms are similar in both types of impact: matrix cracks, fibre failure, debonding at the fibres/matrix interface and delamination. Damage shape on back surfaces is similar after mechanical or laser impacts but differences were detected inside samples.

*Corresponding author: fabienne.touchard@ensma.fr

Originality/value - The combination of these six diagnoses provides complementary information on the damage induced by mechanical or laser impacts in the studied green and synthetic composites.

Keywords - Polymer-matrix composites, Impact loading, Non-destructive testing, Damage

Paper type – Research paper

1. Introduction

The use of lightweight materials is quickly spreading from high performance industrial fields, such as aviation (i.e. composite fuselage of aircrafts), to less demanding ones, such as in energy industry (wind turbine blades), shipyards (parts of yachts), automotive (car parts). In particular, aluminium and carbon fibre reinforced polymers (CFRP) are usually used in aeronautics industry and glass fibre reinforced polymers (GFRP) extensively used for wind turbine blades.

One of the goals in designing and engineering new structures is to make them more environmentally friendly (less CO_2, NO_x emission, low carbon–footprint materials throughout the engineering and life–time cycles). Reducing aircraft mass by replacing aluminium with CFRP and GFRP results in less fuel consumption and gas emission but there are recycling issues when the structure goes out of service. Green composites have been proposed as a viable solution to this new environmental requirement. Such materials are eco–friendly and sustainable, making them a good alternative to classical synthetic composites, in particular GFRP for some semi-structural applications (Corbiere-Nicollier *et al.*, 2001; Joshi *et al.*, 2004; Goutianos *et al.*, 2006; Faruk *et al.*, 2012). As a result, there is a growing interest in the use of natural fibres (hemp, jute, sisal, flax, kenaf, spruce, etc.) or bio-based polymer matrices. They have a lower carbon footprint and their specific properties are comparable to

those of synthetic or mineral fibres due to their much lower density (Wambua *et al.*, 2003; Vasconcellos *et al.*, 2014; Perrier *et al.*, 2016). However, high strain rate behaviour of composites based on natural fibres is not well known yet. In particular, there is still a poor understanding of the response of green composites to impact. The purpose of the present study is to analyse and compare the damage induced by mechanical and laser impacts in a 'green' composite and a glass fibre based one. The research was performed with both non-destructive and destructive evaluation techniques. The investigated systems were prepared and impact damaging was induced by means of a low velocity falling dart machine or by laser shock waves. The induced damage was analysed by six assessment techniques (eye observation, back face relief, terahertz spectroscopy, laser vibrometry, X-ray micro-tomography and microscopic observations) and results were compared.

2. Experimental means

2.1. Investigated materials

Investigations were focused on woven composites based on hemp fibres (assigned symbol: HE1) and glass fibres (assigned symbol: GE1). HE1 is a woven eco-composite, made of 7 plies of plain woven hemp fabric (267±1g/m2) impregnated with epoxy resin EPOLAM 2020 from Axson Technologies. The woven microstructure is based on hemp fibre filaments from plant stem, arranged in yarns with several hemp fibres twisted with a mean angle of 11°. In the fabric, a bundle of three yarns in weft direction is alternated by a bundle of three yarns in warp direction (Fig. 1). The woven hemp/epoxy composite has been manufactured by the vacuum infusion process to obtain plate-like samples. Vacuum infusion involves the infusion of resin into a dry fibrous preform placed on a stiff mould and covered by a flexible membrane (vacuum bag). The second sample (GE1) is a fully synthetic woven composite,

made of 7 plies of plain woven glass fabric impregnated with the same EPOLAM 2020 resin. The planar size of the HE1 and GE1 samples was the same (250 x 250 mm^2) with thickness equal to 4 mm and 2 mm, respectively. In both samples, the 7 woven plies were positioned with the warp yarns oriented in the same direction.

2.2. Laser impacts

The Laser Shock technique is a method to achieve high levels of loading inside the materials. It can be used for damage threshold analyses (Ecault *et al.*, 2014; Ferrante *et al.*, 2015; Perrier *et al.*, 2015) and allows, for example, to simulate space debris and meteoroids impacts (Katz *et al.*, 2008). When the laser beam is directed and focused onto a specimen, it causes the sublimation of the matter on the surface, and the plasma created induces a reaction force in the form of a pressure shock wave that propagates through the material. Then, when the shock wave reaches the back face of the material and meets the air, a release wave is generated in the opposite direction. This release wave encounters the first release wave generated in the front face of the sample at the end of the laser pulse. In this condition the sample is subjected to a high tensile loading state (Ecault *et al.*, 2016). The laser impact tests were performed at the laser facility of PIMM (Paris, France) with the HEPHAISTOS platform (Fig. 2).

All samples were tested at six different laser shock intensities, keeping constant the shock diameter (6 mm) and the pulse duration (10.2 ns). Each sample was laser-impacted in a different independent zone for each laser intensity. The values of energy and intensity for the HE1 and GE1 samples have been collected in Table 1.

2.3 Mechanical impacts

Mechanical impacts were performed by means of a falling dart impact testing machine (Fractovis Plus from CEAST) at IPCB (Naples, Italy). The specimens were tested at different impact energy levels by keeping constant the incident mass at 1.9265 kg and varying the falling height. The impacts were applied by means of a hemispherical impact head (12.7 mm in diameter). During the impact test, the resistive force exerted by the specimen on the striker is measured by a dynamic load cell as a function of time. Striker velocity is then calculated during the impact event. In addition, knowing the striker mass and falling height, the software calculates curves that characterize the impact event.

Both HE1 and GE1 samples were impacted with 1, 2.5 and 5 J energy. The curves recorded during the impact tests are shown in Fig. 3. These diagrams characterize the mechanical behaviour of impacted composites. From load-time curves (Fig. 3a) it is possible to observe that the load increases with an almost linear trend up to a change of the slope, which corresponds to the damage onset (incipient damage point) (Ghasemi and Parvizi, 1990; Herbert *et al.*, 2008; Sarasini *et al.*, 2016). Then, the load reaches a maximum value (peak load) and decreases up to zero.

Displacement versus time curves (Fig. 3b) show that the displacement rises up to a maximum value (maximum displacement) and then it decreases due to the elastic recovery of the composite (it reaches negative values when there is striker rebound). Energy versus time curves (Fig. 3c) reveal that the energy increases up to a maximum value (which corresponds to the impact energy) and then it decreases to a value dependent on the energy dissipation during the impact. Load versus displacement curves (Fig. 3d) show that during the impact test the load first increases with an almost linear trend (stiffness related to the elastic response of

the composite) and then it reaches an onset value corresponding to the inception of damages in the structure. After the maximum deflection is reached, the displacement decreases due to the partial elastic recovery of the composite structure. It is worth to note that the residual displacement (at load equal to zero) is a direct evidence of the damaging occurred in the composite.

The parameters that characterize the mechanical behaviour of impacted composites are evaluated from the impact curves and are displayed in Fig. 4. The Fig. 4a shows that generally the peak load rises with the impact energy, according to literature (Belingardi and Vadori, 2002; De Rosa *et al.*, 2012), until fibre breakage occurs. The maximum displacement (Fig. 4b) and the post-impact (residual) displacement (Fig. 4c) are parameters influenced by the impact energy and by the specific properties of the sample. The elastic recovery and the absorbed energy (Fig. 4d and 4e) are in accordance with the post-displacement values (low post-impact displacement values correspond to low absorbed energy). It can be observed that these parameters generally increase with the impact energy; however, when there is relevant damage, elastic energy shows considerable drop (HE1 sample for 5J). As also confirmed by the scientific literature, linear stiffness values (Fig. 4f) do not change substantially with the increase in the impact energy (Belingardi and Vadori, 2002; De Rosa *et al.*, 2012). In order to compare the composite stiffness between materials, it is worth noting that thickness is different in HE1 (4 mm) and GE1 (2 mm) samples, thus the actual values of parameters can be influenced by the different geometry.

3. Results from assessment techniques

3.1. Naked eye

Front face pictures of laser impacted samples are not presented, because they are covered with an aluminium coating to allow the generation of the shock wave. Relevant pictures of

back surfaces after laser impact are presented in Fig. 5 and 6. Eye observations show visible circular internal damage for HE1 and GE1 samples, in particular from 1.15GW/cm^2. In general, HE1 presents larger damage than GE1 (Fig. 7). Moreover, HE1 presents spallation at 4.46GW/cm^2 (Fig. 5a, Fig. 7).

Relevant pictures of front and back faces after mechanical impact are presented in Fig. 8 (for HE1) and Fig. 9 (for GE1). Damage with circular shape appears on the HE1 front face after the impact at 2.5 J, due to the permanent indentation of the impacted surface under the impactor tip. In the HE1 sample impacted with 5 J impact energy, the front face shows a cross shaped damage. For HE1 composite, back face always shows a cross-shaped damage at all impact energy. Damage path proceeds in 0° and 90° directions, in accordance with the yarn orientation in the fabric (Vasconcellos *et al.*, 2014). On the contrary, GE1 samples showed a white-coloured area denoting internal damage in both back and front surfaces, as a result of a limited damage of the composite.

HE1 shows damage similar to GE1 in front surface after the 1 J and 2.5 J impacts, while a greater damage on the back face occurs after an impact at 5 J (Fig. 10). Damaged areas of front and back faces have been measured as the area of the circle including the visible damage. The damage area increases with the increasing impact energy. As typical the damaged areas on back surfaces are bigger than the ones on front surfaces and HE1 samples show larger damage than GE1 ones.

3.2. Back face relief

Further observations of the samples were performed at PPRIME Institute (Poitiers, France) with multidimensional image acquisitions by means of a ZEISS Axio Imager Vario Z2 microscope and the AxioVision Imaging System software. AxioVision captures images for a range of equally spaced focus positions, allowing imaging of rough surfaces and making

3D reconstructions. With this information, it is possible to characterize the superficial damage induced on samples and compare their depth and geometry with other materials.

Multidimensional images for selected impacts have been captured in order to visualize the 3D surface profiles of back face damage. After laser impact, there is no measurable back face relief (BF relief) in GE1 sample. HE1 after laser impact presents measurable damage only in the case of spallation. The corresponding 3D reconstruction and damage profile are shown in Fig. 11a. Length and maximum height measured in back face relief are plotted as a function of laser impact energy in Fig. 12a and 12b.

HE1 and GE1 after mechanical impacts show an irregular geometry after the impact at 5J, while no detectable changes in depth after the impact at 1J were detected (Fig. 11b). GE1 was the only system showing some detectable change in back face depth after the impact at 2.5 J, while HE1 did not show appreciable variations. This can be probably due to the different thickness of HE1 and GE1 samples (4 mm and 2 mm respectively), which can affect the back face impact response. Length and maximum height measured in back face relief are plotted as a function of mechanical impact energy in Fig. 12c and 12d.

3.3. Terahertz spectroscopy

Terahertz time domain spectroscopy uses electromagnetic radiation in the terahertz range, covering frequencies between 100 GHz and 10 THz. It is employed in several applications like medicine, biology, security and non-destructive testing. Unlike X-rays, THz waves do not present a health risk (the photon energy is very low, therefore they are non-ionizing) (Chiou *et al.*, 2009). The characteristic material response to terahertz irradiation are a high transparency in case of dielectrics and a high reflectivity in case of conductive materials (such as metals and water). At each dielectric interface, e.g. from air to the composite material, the electromagnetic waves experience partial transmission and reflection (Beigang *et al.*, 2016).

This radiation can be used to identify defects in samples and abnormalities from foreign material inclusions, debonding and delamination, impact damage, heat damage, and water or hydraulic fluid ingression (Zhang and Xu, 2009). The results presented here were obtained using the Teraview TPS Spectra 3000 at IMP-PAN (Gdansk, Poland). The samples were measured from one side registering reflections (C-scans) in a very dense number of points.

Relevant C-Scan images of laser impacted samples are presented in Fig. 13a (HE1 sample) and Fig. 13b (GE1 sample). Impacted areas are evidenced with circles. This technique did not allow the identification of any impact point in either GE1 or HE1 system. Only the impact at 4.46GW/cm^2 (no. 34; HE1 sample) was detected.

The analysis performed on mechanically impacted samples clearly identified the impact points. In particular, in Fig. 14, C-scans at selected time slices for HE1 samples show the experimental evidences of damaging after all impacts.

3.4. Vibrometry

Laser Doppler Vibrometry is a contactless technology that directly measures the vibration velocity of an object surface using a laser beam (Ostachowicz *et al.*, 2012). It allows registering vibrations as well as propagating elastic waves. Measurements can be performed for dense grid allowing visualising the vibration phenomena. The laser vibrometer uses a "point and shoot" technology: the piezoelectric element generates an excitation pulse and the scanning head measures the velocity of vibration in a selected point. This procedure is repeated in all points of the created grid, in order to monitor the propagation of the guided elastic waves through the sample. Vibrometry analysis was performed at IMP-PAN (Gdansk, Poland). In order to excite the samples a piezoelectric disc glued to the inspected samples was used (0.5 mm thick and 10 mm in diameter). Samples were placed on 2cm thick polyurethane foam to reduce the influence of external vibrations on the measurement and to simulate free

vibration conditions. The assessment of the samples was based on calculation of the root mean square (RMS) value for each point. RMS values are different in damaged and non-damaged points because guided elastic waves are altered at damage location (Radzienski *et al.*, 2011).

RMS values for laser impacted samples are depicted in Fig. 15a and 15b for HE1 and GE1 samples, respectively. The highest RMS values are located in the vicinity of the piezoelectric sensors, being the source of waves. There are some impact areas with noticeable changes in RMS values, which indicates the presence of damage. Besides, in some impact areas without variations in RMS map the wave propagation animation shows little alterations, revealing the existence of small damages. In case of HE1 sample, the impact no. 34 was clearly detected while the impact no. 35 gave only a slight variation of the small response. In the case of the GE1 sample, only the highest intensity impact (no. 22) was detected.

The laser vibrometry results for mechanically impacted samples are presented in Fig. 16a and 16b for HE1 and GE1 samples, respectively. The highest RMS values still indicate the piezoelectric sensor location. For both materials, the 5 J impact was detected, while the 2.5J is visible only for GE1 sample.

3.5. Tomography

Tomography (or Computerized Axial Tomography, CT) is a non-destructive technique for the study of the physics and mechanics of materials, given its great ability to analize the internal microstructure of a material. The basis of this technique is the reconstruction of three-dimensional volumes from a sequence of projection images (generally obtained from an exposition to an X-Ray beam) taken at different equally spaced angles around the object. The result of the reconstruction is a series of images (slices) at different consecutive sections along one or more axes (Landis and Keane, 2010). The base principle under tomography imaging is

related to the X-Ray absorption physics. Light absorption in a material is a logarithmic function of its absorption capacity and of the distance that it must travel (Beer–Lambert law). Light absorption decreases when the energy of the X-Ray photons increases. In general, for a fixed X-Ray photon energy, elements with a smaller atomic number absorb less radiation than higher atomic number elements. In a 3D tomography image, a voxel, or volumetric pixel, represents the X-Ray absorption of the material in that position. This means that the reconstruction of the X-Ray projections provides a three-dimensional spatial distribution (3D map) of the X-Ray absorption capability of the material. Given the fact that different phases (or characteristics) of a material have different absorption capacities, these can be easily identified by means of the mentioned three-dimensional map. Image acquisition has been performed at PPRIME Institute (Poitiers, France) using an UltraTom CT scanner manufactured by RX Solutions (France). This piece of equipment makes possible the collection of images up to a 0.25 μm in resolution (RX Solutions website, 2016). A 12 μm resolution has been used in this work.

Laser impacted HE1 sample presents spallation at 4.46GW/cm^2 (impact no. 34). Matrix cracks, fibre failure and cracks at the yarn/matrix interface have been detected in the tomographic images (Fig. 17a). In the case of the 2.24GW/cm^2 impact (no. 35) matrix cracks and cracks at the yarn/matrix interface have been observed near the back face (Fig. 17b). Tomographic images of laser impacted GE1 samples were performed for several levels of intensity (no. 22 for 4.55GW/cm^2, no. 23 for 2.25GW/cm^2, no. 24 for 1.15GW/cm^2, no. 25 for 0.60GW/cm^2). In all cases no damage has been clearly detected (Fig. 17c).

Among all mechanically impacted samples, HE1 and GE1 at 2.5J were analysed (Fig. 18). For the HE1 sample (Fig. 18a), the tomographic image in the X-Y plane shows that damage proceeds in preferential directions, along the warp and weft directions of the woven fabric. In accordance with literature (Shyr and Pan, 2003; Petit *et al.*, 2007), a conical pattern

of damage in the thickness direction has been detected, enlarging from the impacted front face towards the back face. Fig. 18a also shows the presence of matrix cracks and debonding at the fibres/matrix interface. Furthermore, a yarn failure near back face can be observed. In the case of the GE1 sample impacted at 2.5J, tomographic images present a clear damage near the back face while fibre breakage and matrix cracks can be observed in the Z-direction of the reconstructed volume (Fig. 18b).

3.6. Optical microscopy

The failure mechanisms generated by the impacts on the composites were also observed using a Reichert-Jung optical microscope. For this type of observations, samples had to be accurately prepared to allow the correct detection of fine details. Samples were carefully cut, in order to avoid contamination or development of new damage. A FINOCUT Low Speed Precision Cutter by METKON was used to prepare all samples intended for microscopic observations. After cutting, specimens surfaces were polished by using a Struers RotoPol-31 equipment. Finally, samples were embedded in a resin to ease their grip during polishing and then underwent optical microscopic observation.

HE1 sample, damaged by means of the laser shock wave technique set at 2.24GW/cm^2 (no. 35), showed matrix cracks and cracks at the yarn/matrix interface near the back face (Fig. 19a). Microscopic observations carried out on the GE1 sample performed on the no. 22 impact (executed at 4.55GW/cm^2), showed debonding at the fibres/matrix interface and delaminations (Fig. 19b).

Microscopic observations were also carried out on the mechanically impacted GE1 sample at 1J (Fig. 20). Areas with cracks at the fibres/matrix interface and delamination were largely identified. Near back face, no damage was detected.

4. Discussion and conclusions

The several techniques used in order to detect the damage type and extension and to analyse the damaging mechanisms occurring during an impact on laminated composites allowed to identify the damaging with different sensitivities, and different thresholds were detected (Fig. 21). The comparison of the different techniques shows that naked eye observation, back face relief and tomography permitted to identify spallation, while THz spectroscopy and vibrometry allowed the identification of damages but weren't able to distinguish spallation from the other types of damages (Fig. 21c and 21d).

In regard to mechanically impacted composites (Fig. 21a and 21b), it is observed that generally both eye observation and THz technique allowed to detect damage at lower energies than back face relief and vibrometry. In particular, damages induced by applying a 1J impact on GE1 sample can only be detected by eye observation. Eye observation resulted to be the most sensitive technique also for laser impacted samples (Fig. 21c and 21d), allowing the determination of low intensity damages with respect to the other non-destructive techniques.

Although eye observation, back face relief, THz and Vibrometry showed a good capability to detect and locate damages, they didn't present enough precision for the analysis of damage mechanisms. For this purpose, X-ray micro-tomography and microscopic observations were the only techniques able to clearly investigate the response of the internal structure. X-ray micro-tomography acquires images of the whole sample in the three planes, while optical microscopy, being a destructive technique, enables to analyse only few sections of the sample. On the other hand, images obtained by microscopic observations are characterized by a higher resolution and finer details can be detected, also thanks to the higher degree of magnifications available.

Damage induced by mechanical and laser impacts showed relevant differences in the position of damages. In laser impacted samples, the damage was induced near the back face.

In mechanically impacted samples, damage appears close to the front face and then propagates towards the back face (Fig. 22). The observed damage mechanisms were instead similar for both types of impacts. In fact, both mechanical and laser impacted composites exhibited matrix cracks, fibre failure, debonding at the fibres/matrix interface and delamination. The shape of the damage on the back surfaces is similar after mechanical or laser impacts. There are white circular areas denoting internal damage. The exception is the mechanically impacted HE1 sample, which presents a cross-shaped damage propagating in 0° and 90° (orientation of the fibres). This behaviour could be due to the different types of loading occurring in the composite structures during the impact events. In fact, because of the very short duration of the laser shock, the stress during laser impacts is essentially due to the shock wave, while a complex combination of stresses created by the shock wave and structural effects (as the bending phenomenon) are induced in the sample by the indenter during mechanical impacts.

5. Acknowledgments

This study was realised thanks to a French-Polish-Italian collaboration in the frame of the project “Eco-Composites: damage Analysis Using Laser shock Technology” (PICS “ECAULT”– No. 6366).

6. References

Beigang, R. *et al.* (2016), Technische Universität Kaiserslautern. Ultrafast Photonics and THz Physics Group, available at: http://www.physik.uni-kl.de/en/beigang/forschungsprojekte/ (accessed January 2016).

Belingardi, G. and Vadori, R. (2002), “Low velocity impact tests of laminate glass-fiber-epoxy matrix composite material plates”, *International Journal of Impact Engineering*, Vol. 27, pp. 213-229.

Bonnafous, C., Touchard, F., Chocinski-Arnault, L. (2011), "Damage mechanisms in hemp-fibre woven fabric composites and comparison with glass-fibre composite." *Polymers and Polymer Composites*, Vol. 19, No. 7, pp. 543-552.

Chiou, C.P., Blackshire, J.L., Thompson, R.B., Hu, B.B. (2009), “Terahertz ray system calibration and material characterizations”, *Review of QNDE*, Vol. 28, pp. 410-417.

Corbiere-Nicollier, T., Gfeller Laban, B., Lundquist, L., Leterrier, Y., Månson, J.-A.E., Jolliet, O. (2001), “Life cycle assessment of biofibres replacing glass fibres as reinforcement in plastics”, *Resources, conservation and recycling*, Vol. 33, pp. 267-287.

De Rosa, I. M., Dhakal, H. N., Santulli, C., Sarasini, F., Yi Zhang, Z. (2012), “Post-impact static and cyclic flexural characterisation of hemp fibre reinforced laminates”, *Composites Part B*, Vol. 43, pp. 1382-1396.

Ecault, R., Boustie, M., Berthe, L., Touchard, F., Chocinski-Arnault, L., Voillaume, H., Campagne, B. (2014), “Developments of a laser shock wave adhesion test on bonded CFRP composites”, *International Journal of Structural Integrity*, Vol. 5, No. 4, pp. 253-261.

Ecault, R., Touchard, F., Boustie, M., Berthe, L., Dominguez, N. (2016), “Numerical modeling of laser-induced shock experiments for the development of the adhesion test for bonded composite materials”, *Composite Structures*, Vol. 152, pp.382-394.

Faruk, O., Bledzki, A.K., Fink, H.-P., Sain, M. (2012), “Biocomposites reinforced with natural fibers: 2000–2010”, *Prog. Polym. Sci.*, Vol. 37, pp. 1552–1596.

Ferrante, L., Tirillo, J., Sarasini, F., Touchard, F., Ecault, R., Vidal Urriza, M.A., Chocinski-Arnault, L., Mellier, D. (2015), "Behaviour of woven hybrid basalt-carbon/epoxy composites subjected to laser shock wave testing: preliminary results", *Composites Part B*, Vol. 78, No. 1, pp. 162-173.

Ghasemi, N., Parvizi, M. (1990), "Impact behaviour and damage tolerance of woven carbon fibre-reinforced thermoplastic composites", *Composites*, Vol. 21, No. 2, pp. 155-168.

Goutianos, S., Peijs, T., Nystrom, B., Skrifvars, M. (2006), "Development of Flax Fibre based Textile Reinforcements for Composite Applications", *Appl. Compos. Mater.*, Vol. 13, pp. 199–215.

Hebert, M., Rousseau, C., Shukla, A. (2008), "Shock loading and drop weight impact response of glass reinforced polymer composites", *Composites Structures*, Vol. 84, pp. 199-208.

Joshi, S.V., Drzal, L.T., Mohanty, A.K., Arora, S. (2004), "Are natural fiber composites environmentally superior to glass fiber reinforced composites?", *Composites Part A: Applied Science and Manufacturing*, Vol. 35, No. 3, pp. 371-376.

Katz, S., Grossman, E., Gouzman, I., Murat, M., Wiesel, E., Wagner, H.D.(2008), "Response of composite materials to hypervelocity impact", *International Journal of Impact Engineering*, Vol. 35, pp. 1606–1611.

Landis, E.N. and Keane, D.T (2010), "X-ray microtomography", *Mater. Charact.*, Vol. 61, No. 12, pp. 1305–1316.

Ostachowicz, W., Kudela, P., Krawczuk, M., Zak, A., (2012), "Three-Dimensional Laser Vibrometry", in Guided Waves in Structures for SHM, Wiley, pp. 93-124.

Perrier, A., Ecault, R., Touchard, F., Vidal Urriza, M., Baillargeat, J., Chocinski-Arnault, L., Boustie, M. (2015),"Towards the development of laser shock test for mechanical characterisation of fibre/matrix interface in eco-composite", *Polymer Testing*, Vol. 44, pp. 125-134.

Perrier, A., Touchard, F., Chocinski-Arnault, L., Mellier, D. (2016), "Mechanical behaviour analysis of the interface in single hemp yarn composites: DIC measurements and FEM calculations." *Pol. Testing*, Vol. 52, pp. 1-8.

Petit, S., Bouvet, C., Bergerot, A., Barrau, J. (2007), "Impact and compression after impact experimental study of a composite laminate with a cork thermal shield", *Composites Science and Technology*, Vol. 67, pp. 3286–3299.

Radzienski, M., Dolinski, L., Krawczuk, M., Zak, A., Ostachowicz, W. (2011), "Application of RMS for damage detection by guided elastic waves", *Journal of Physics: Conference Series*, Vol. 305, 012085.

RX Solutions (2016), "UltraTom Système de Tomographie Ultra-Performant", available at: http://media.wix.com/ugd/56ca9d_8eb03ff6c673b5a72514e410c2afd9d9.pdf (accessed January 2016).

Sarasini, F., Tirillò, J., D'altilia, S., Valente, T., Santulli, C., Touchard, F., Chocinski-Arnault, L., Mellier, D., Lampani, L., Gaudenzi, P. (2016), "Damage tolerance of carbon/flax hybrid composites subjected to low velocity impact", *Comp. Part B*, Vol. 91, pp. 144-153.

Shyr, T.W. and Pan, Y.H. (2003), "Impact resistance and damage characteristics of composite laminates", *Composite Structures*, Vol. 62, pp. 193–203.

Vasconcellos, D., Sarasini, F., Touchard, F., Chocinski-Arnault, L., Pucci, M., Santulli, C., Tirillò, J., Iannace, S., Sorrentino, L. (2014), "Influence of low velocity impact on fatigue behaviour of woven hemp fibre reinforced epoxy composites", *Composites Part B*, Vol. 66, pp. 46-57.

Vasconcellos, D., Touchard, F., Chocinski-Arnault, L. (2014), "Tension-tension fatigue behaviour of woven hemp fibre reinforced epoxy composite: a multi-instrumented damage analysis", *International Journal of Fatigue*, Vol. 59, pp. 159-169.

Wambua, P., Ivens, J., Verpoest, I. (2003), "Natural fibres: can they replace glass in fibre reinforced plastics?", *Composites Science and Technology*, Vol. 63, No.9, pp. 1259–1264.

Zhang, X. C. and Xu, J. (2009), *Introduction to THz wave photonics*, Springer.

Table 1. Energy and intensity of laser impact tests

Laser impact no	Sample	Laser energy (J)	Intensity (GW/cm^2)
22	GE1	13.12	4.55
23	GE1	6.49	2.25
24	GE1	3.32	1.15
25	GE1	1.73	0.60
26	GE1	0.78	0.27
27	GE1	0.46	0.16
34	HE1	12.86	4.46
35	HE1	6.47	2.24
36	HE1	3.31	1.15
37	HE1	1.70	0.59
38	HE1	0.77	0.27
39	HE1	0.45	0.16

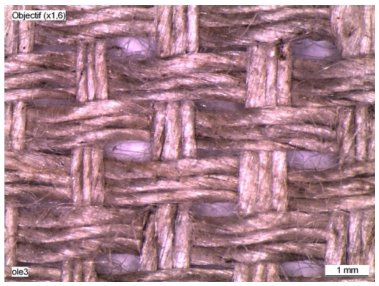

Figure 1. Hemp fabric of the HE1 sample (Bonnafous *et al.*, 2011).

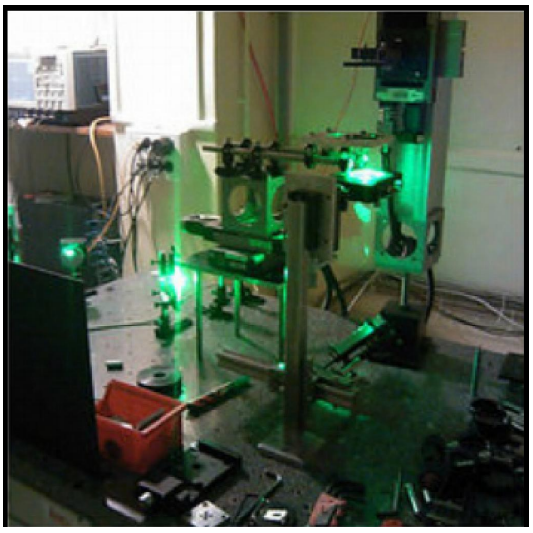

Figure 2. HEPHAISTOS laser facility

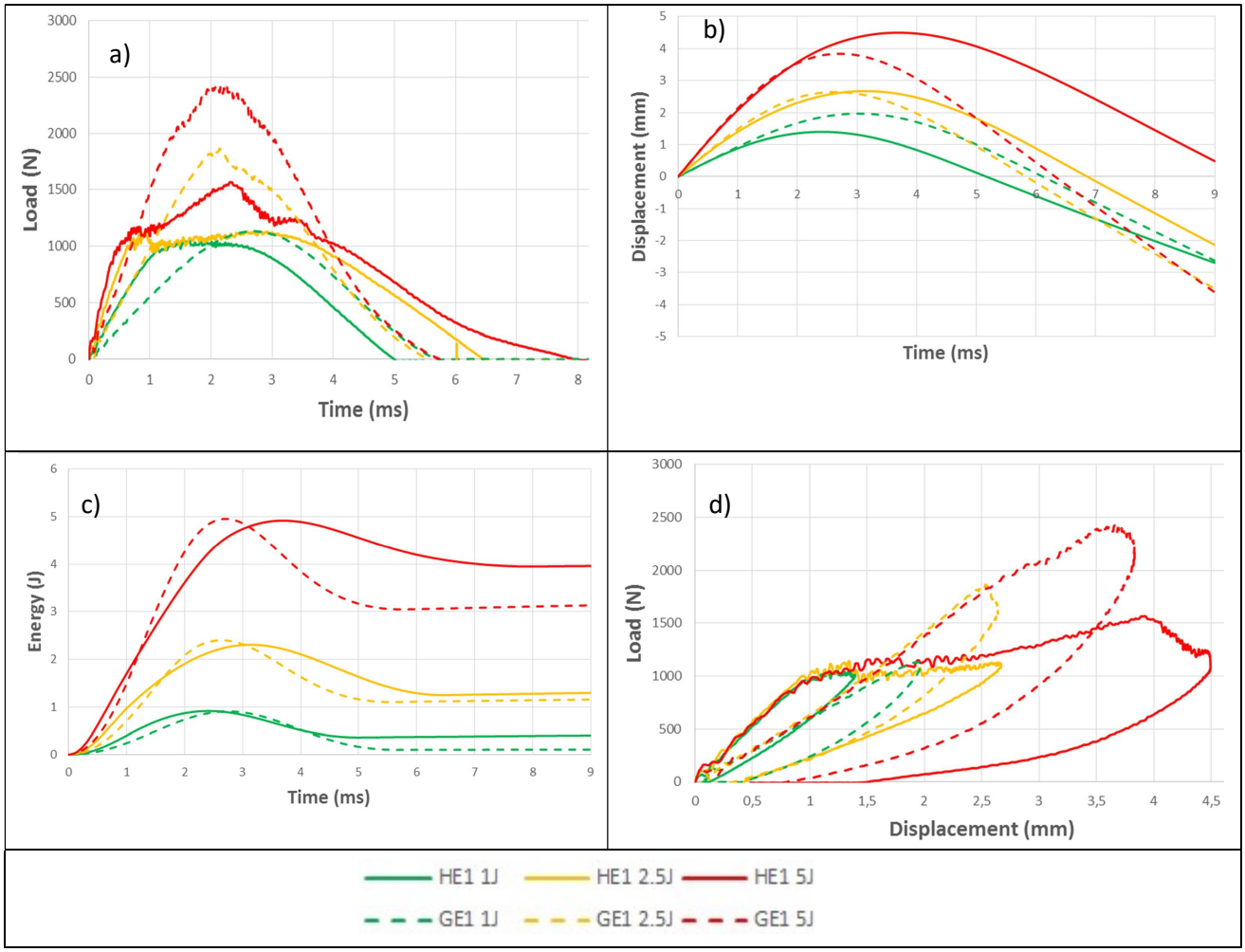

Figure 3. Mechanical impact test curves for HE1 and GE1 samples: a) Load-Time curve, b) Displacement-Time curve, c) Energy-Time curve, d) Load-Displacement curve.

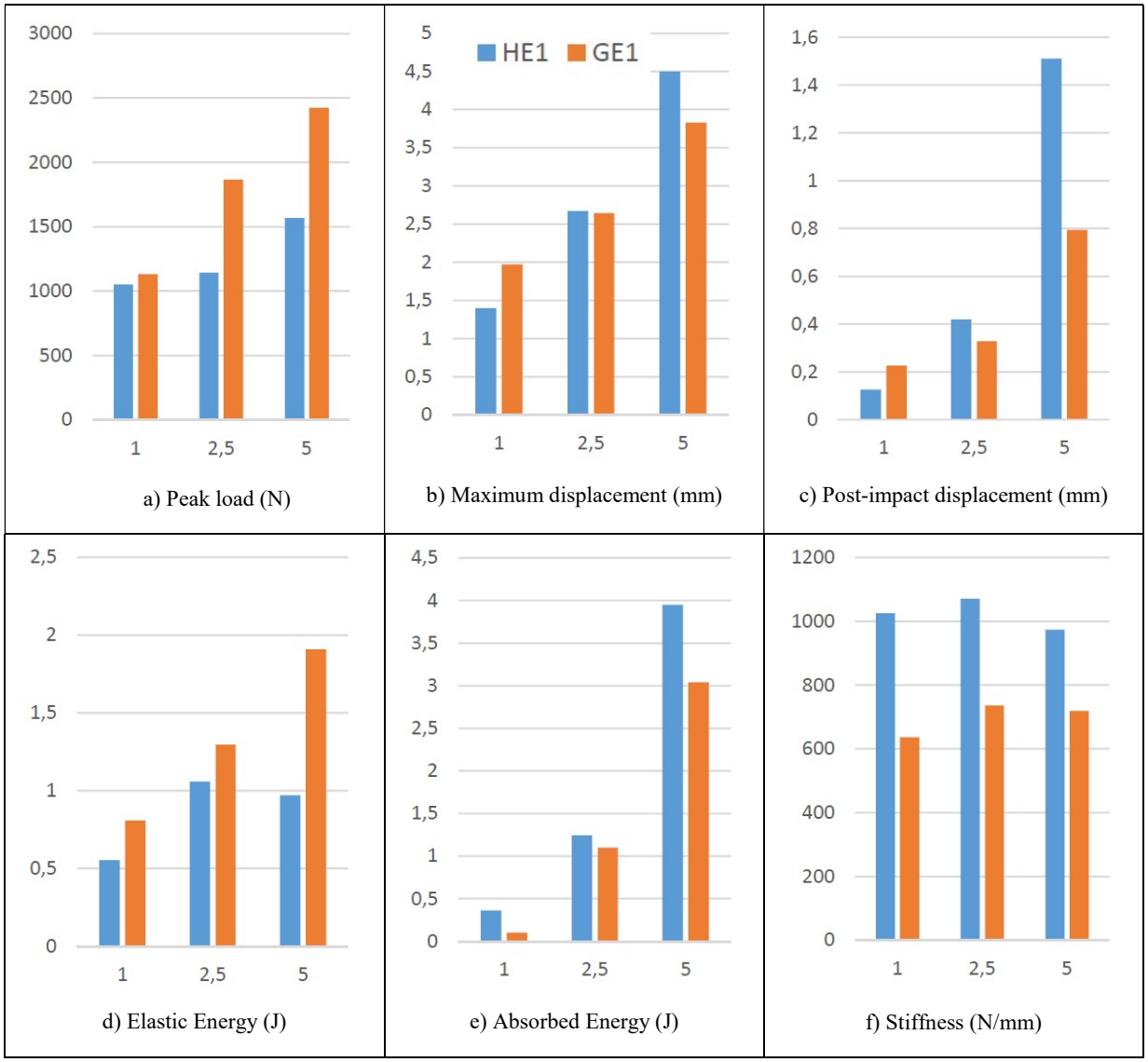

Figure 4. Parameters characterizing the mechanical behaviour of impacted composites measured from the falling dart impact curves.

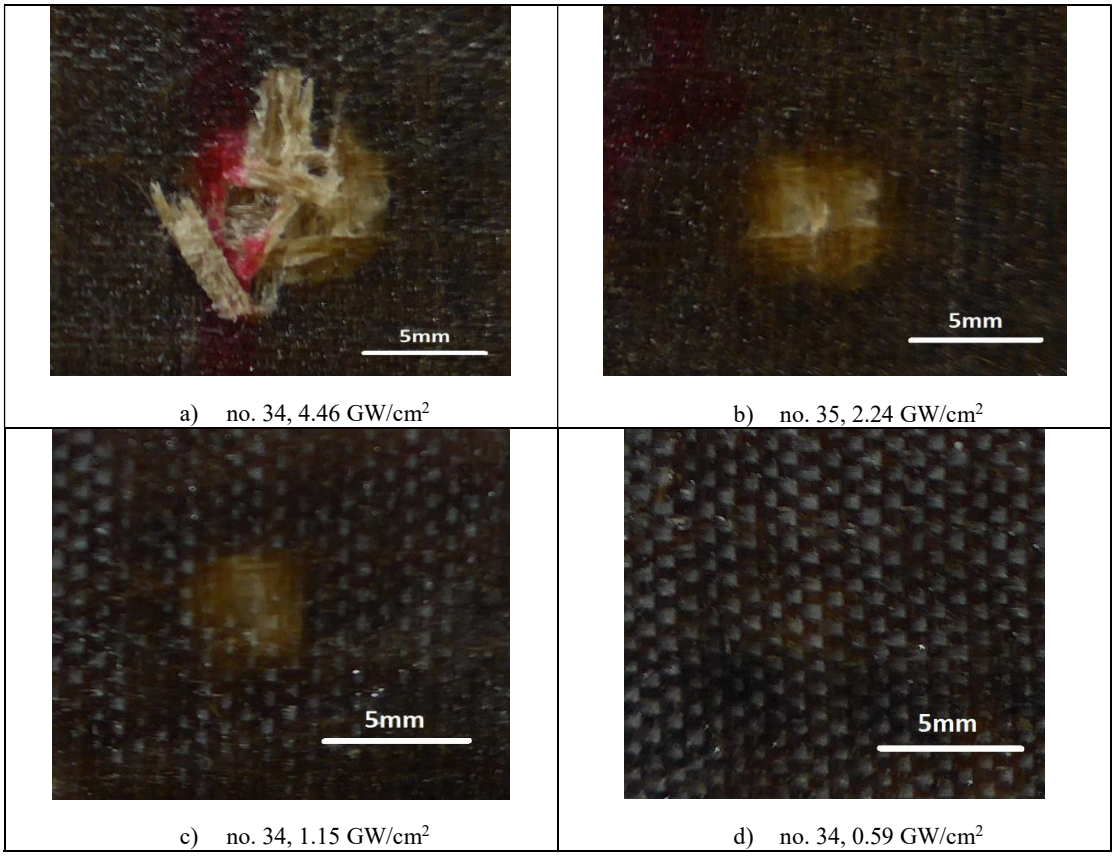

a) no. 34, 4.46 GW/cm^2 b) no. 35, 2.24 GW/cm^2

c) no. 34, 1.15 GW/cm^2 d) no. 34, 0.59 GW/cm^2

Figure 5. Back face pictures after laser impact on HE1 sample

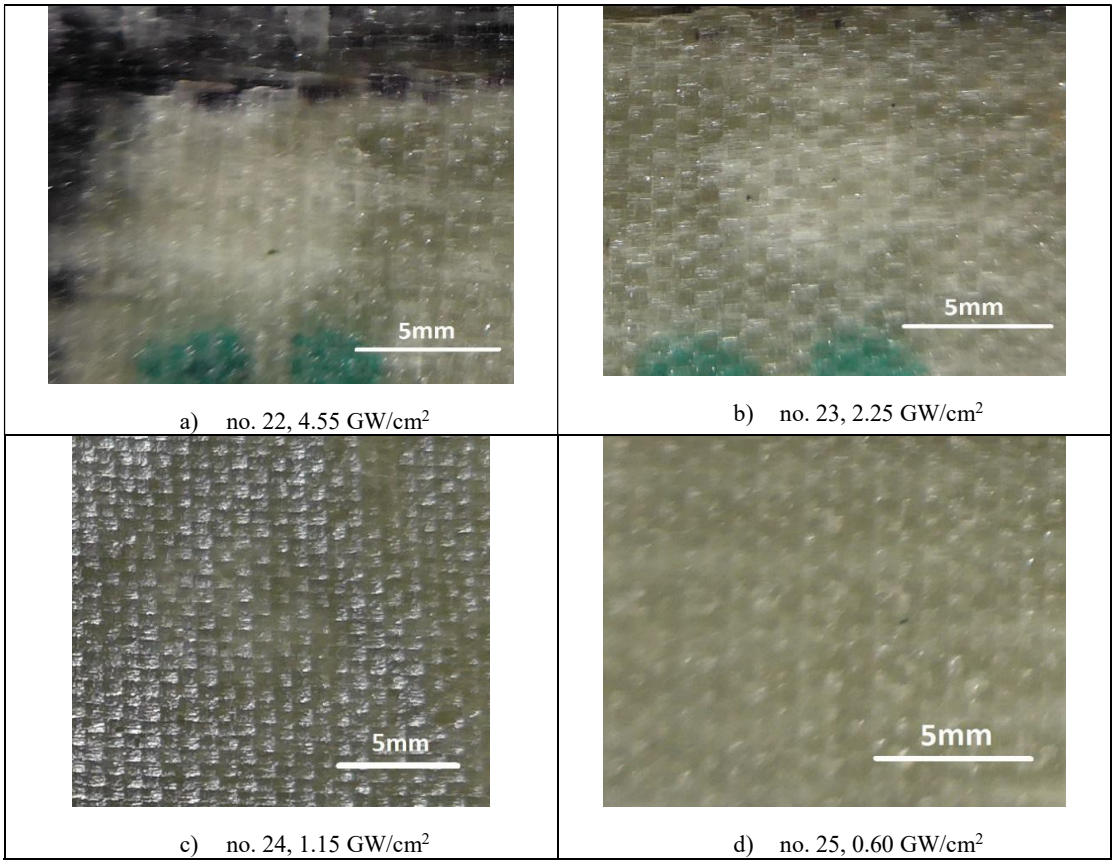

a) no. 22, 4.55 GW/cm^2

b) no. 23, 2.25 GW/cm^2

c) no. 24, 1.15 GW/cm^2

d) no. 25, 0.60 GW/cm^2

Figure 6. Back face pictures after laser impact on GE1 sample

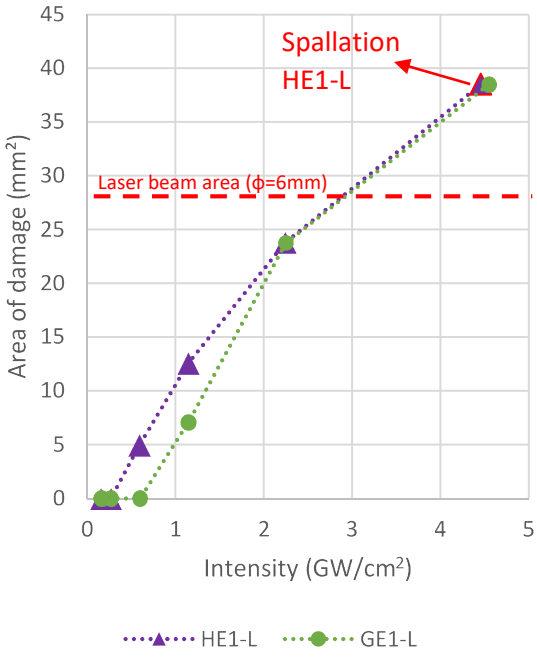

Figure 7. Area of damage – Back face of HE1 and GE1 after laser impacts

e) front face, 2.5J

f) back face, 2.5J

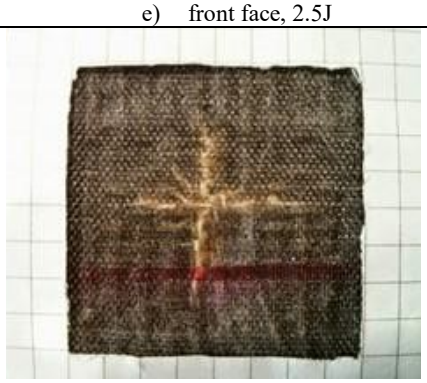

g) front face, 5J

h) back face, 5J

Figure 8. Front and back face pictures after mechanical impact on HE1 sample

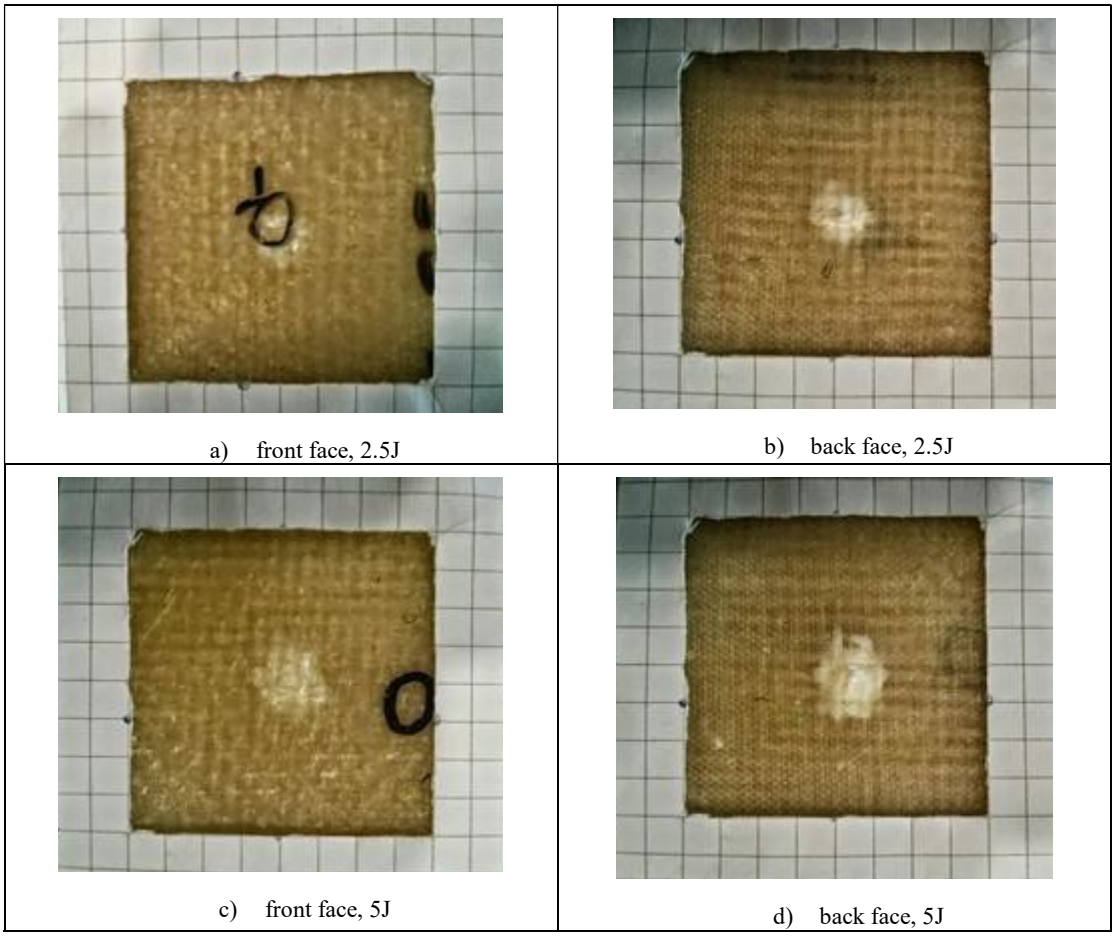

a) front face, 2.5J

b) back face, 2.5J

c) front face, 5J

d) back face, 5J

Figure 9. Front and back face pictures after mechanical impact on GE1 sample

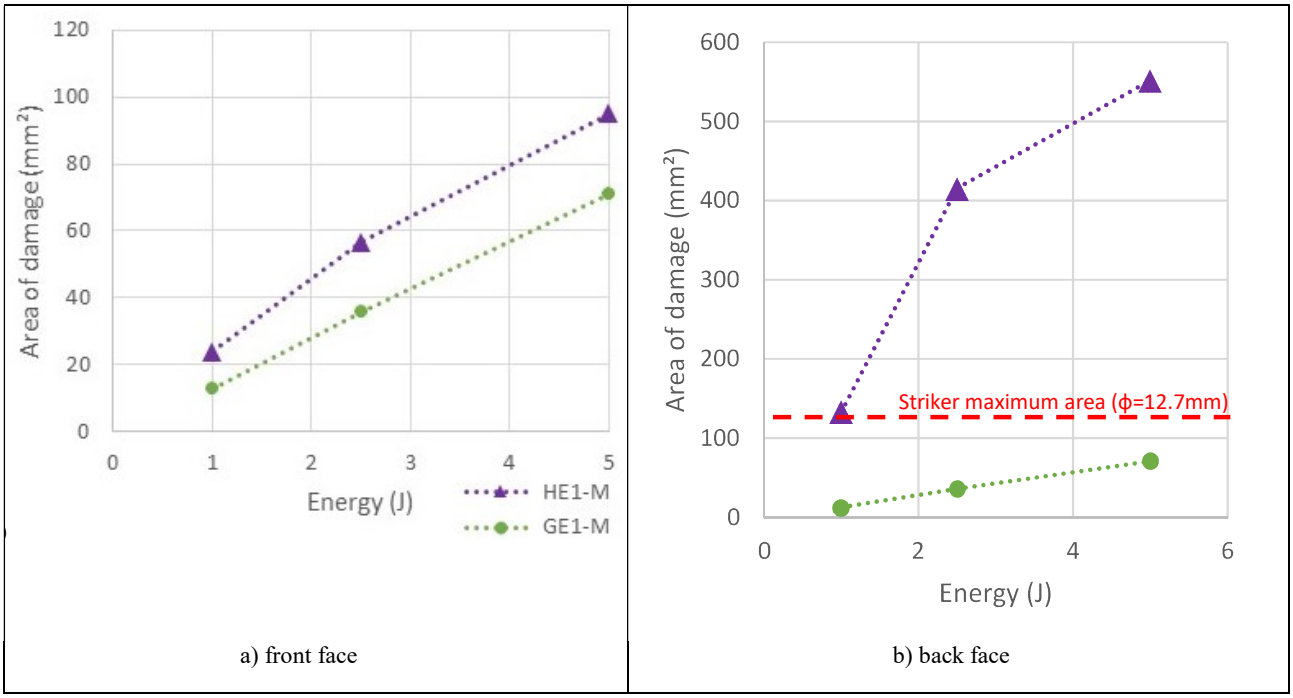

a) front face

b) back face

Figure 10. Area of damage at the front and back faces after mechanical impacts

a)

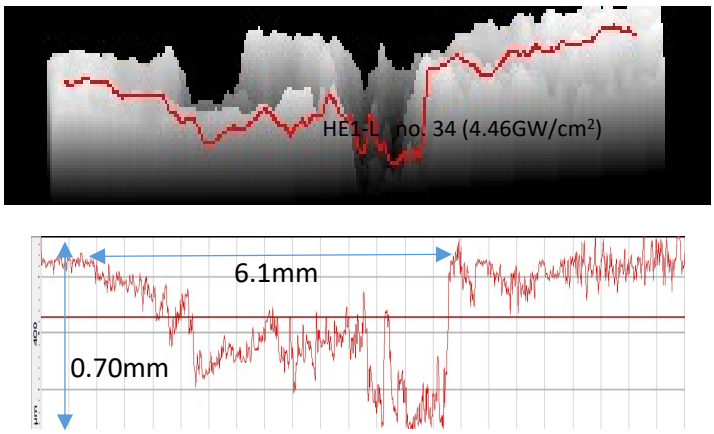

b)

	HE1-M	GE1-M
5J	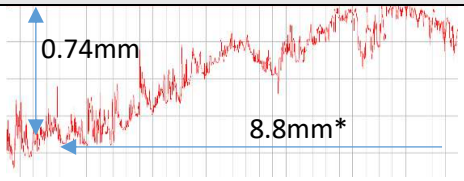	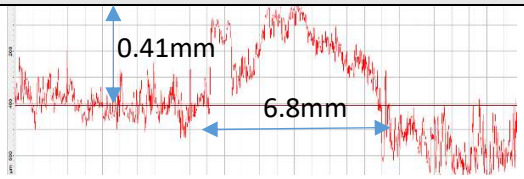
2.5 J	NOT APPRECIABLE	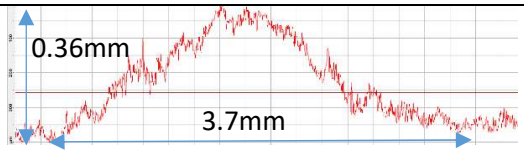
1J	NOT APPRECIABLE	NOT APPRECIABLE

*(Some impacts are partially captured because of their great damage size)

Figure 11. a) 3D reconstruction and z(x) back face profile of laser impact HE1-L no.34 (4.46GW/cm²), b) z(x) back face profiles of HE1 and GE1 samples after mechanical impacts.

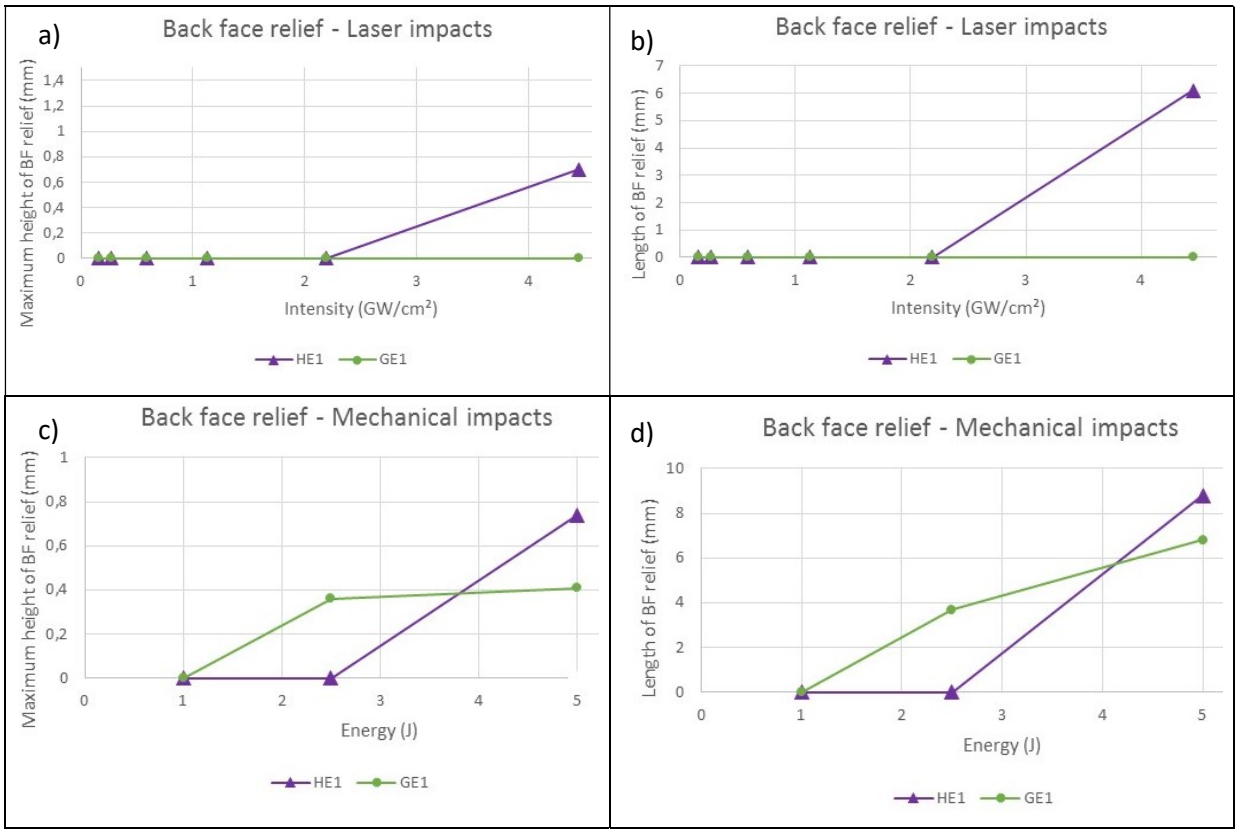

Figure 12. Back face relief – After laser impacts: maximum height (a) and length (b), after mechanical impacts: maximum height (c) and length (d).

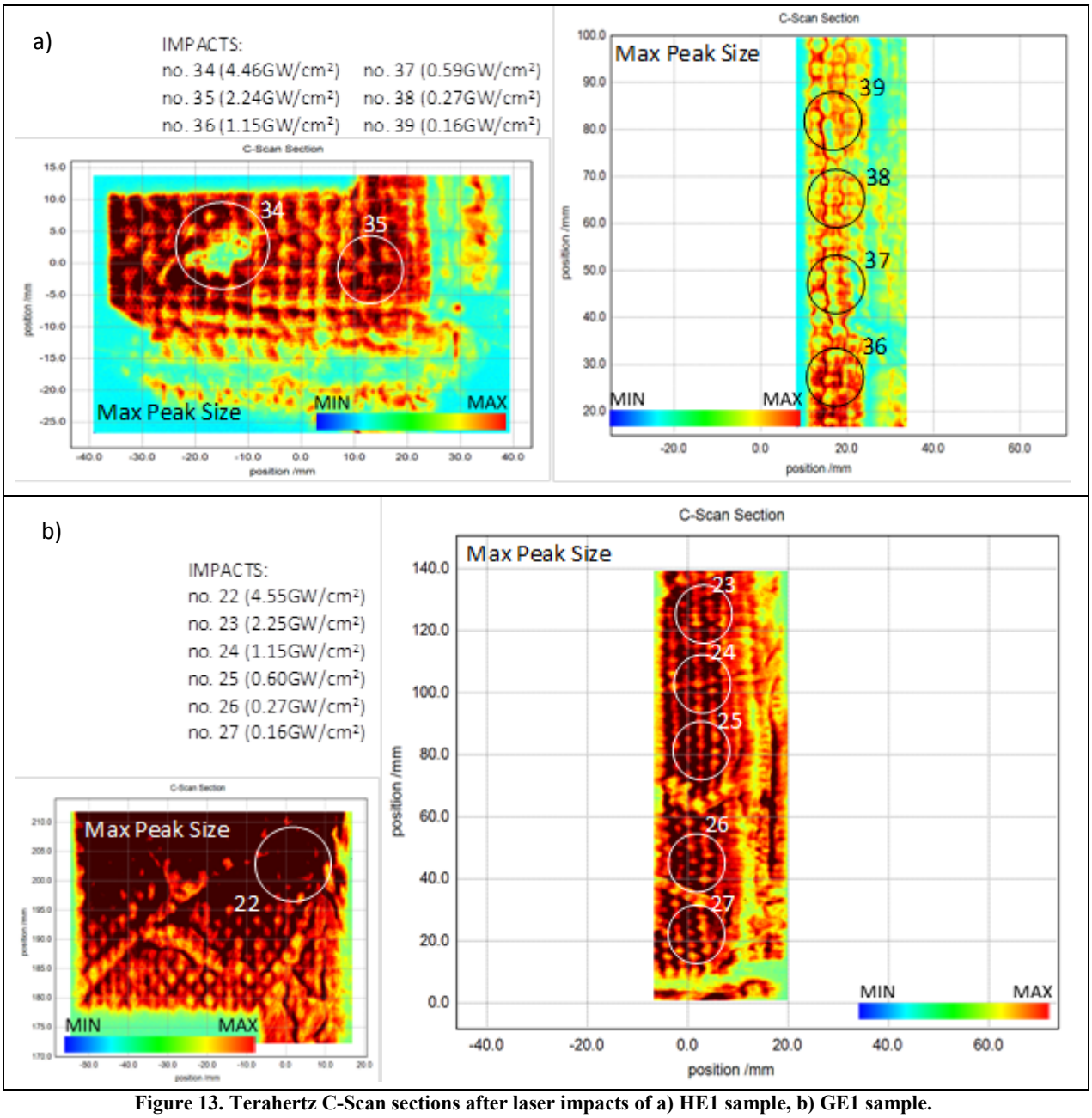

Figure 13. Terahertz C-Scan sections after laser impacts of a) HE1 sample, b) GE1 sample.

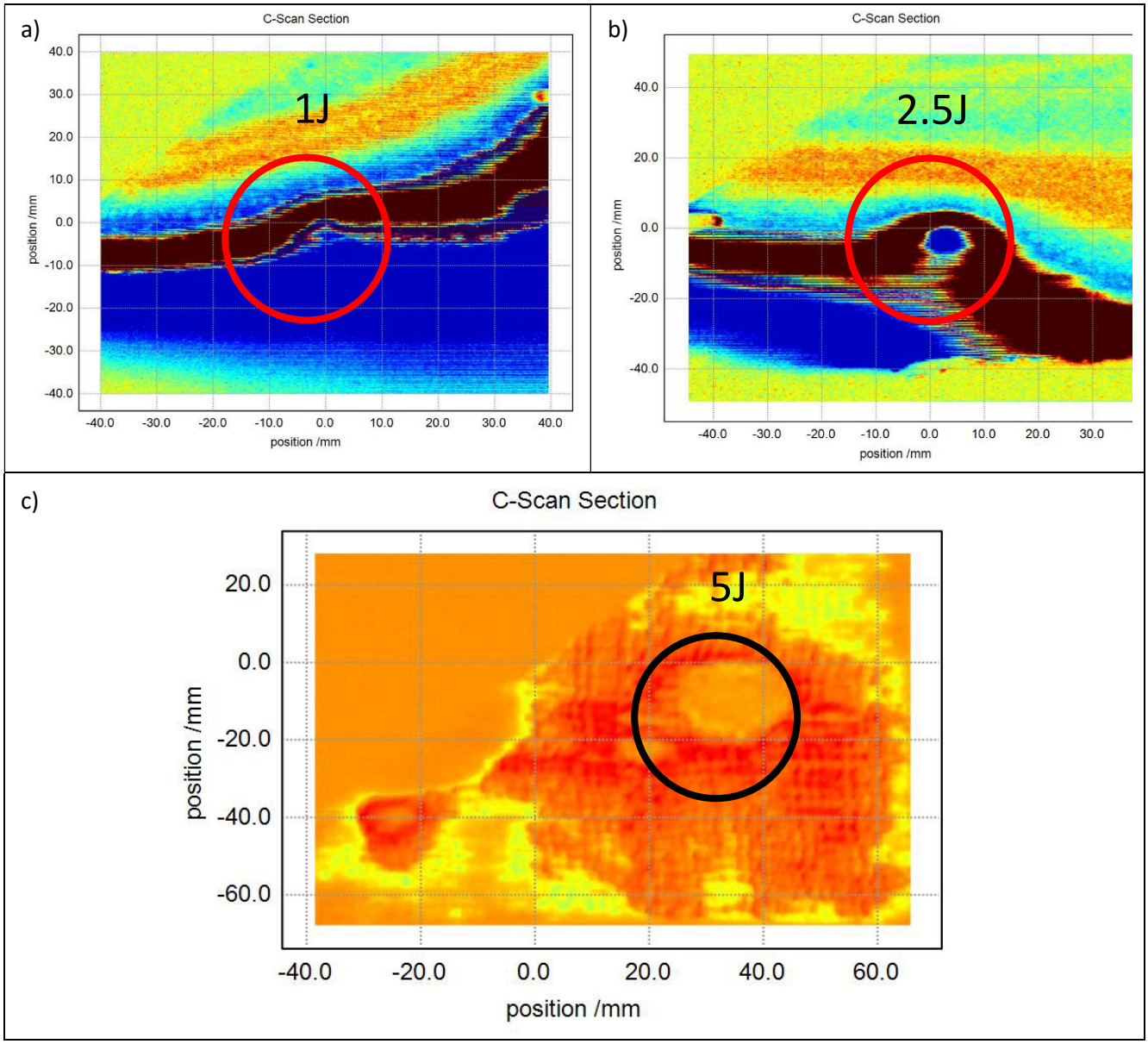

Figure 14. Terahertz C-Scan sections of HE1 at a) 1J impact area, b) 2.5J impact area and c) 5J impact area.

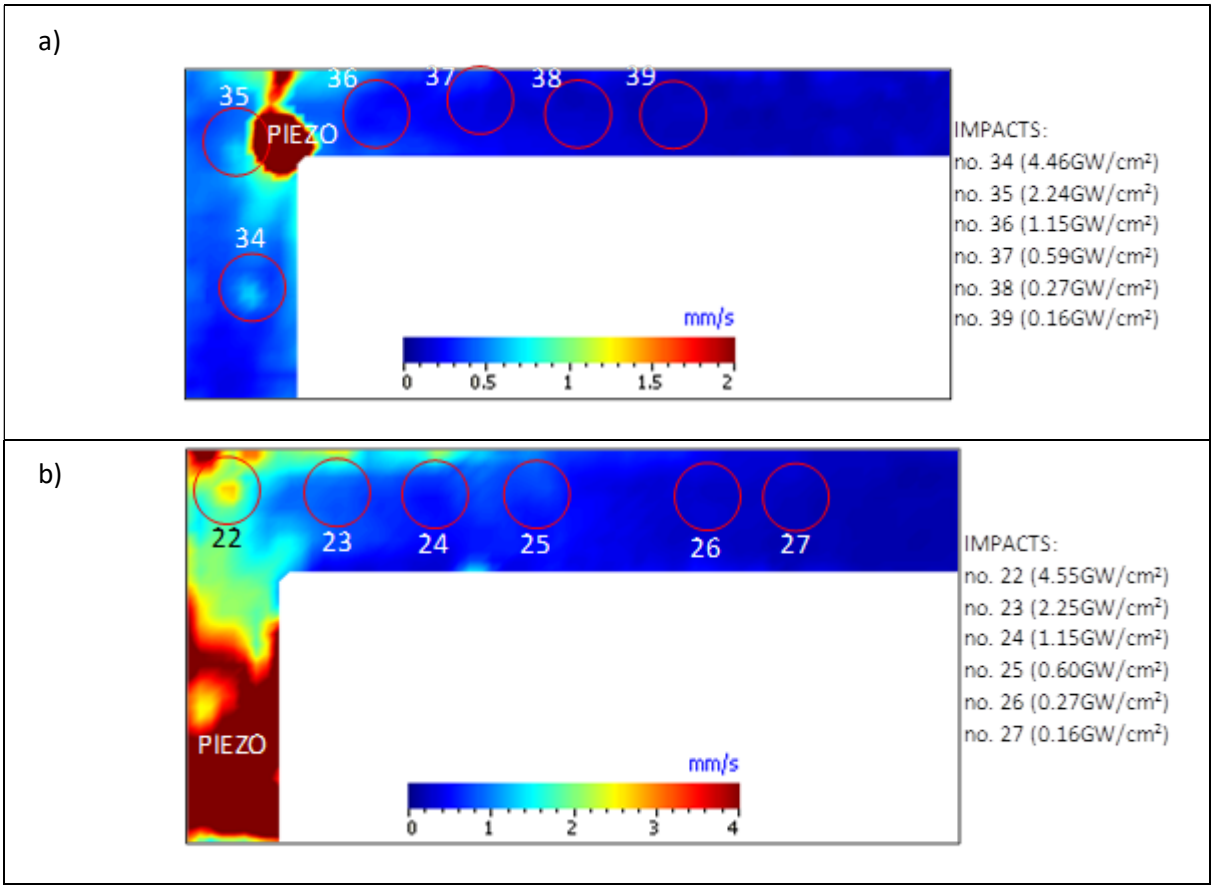

Figure 15. RMS values for a) HE1 sample (frequency of excitation: 100 kHz, voltage: 400 Vpp), b) GE1 sample (frequency of excitation: 200 kHz, voltage: 400 Vpp).

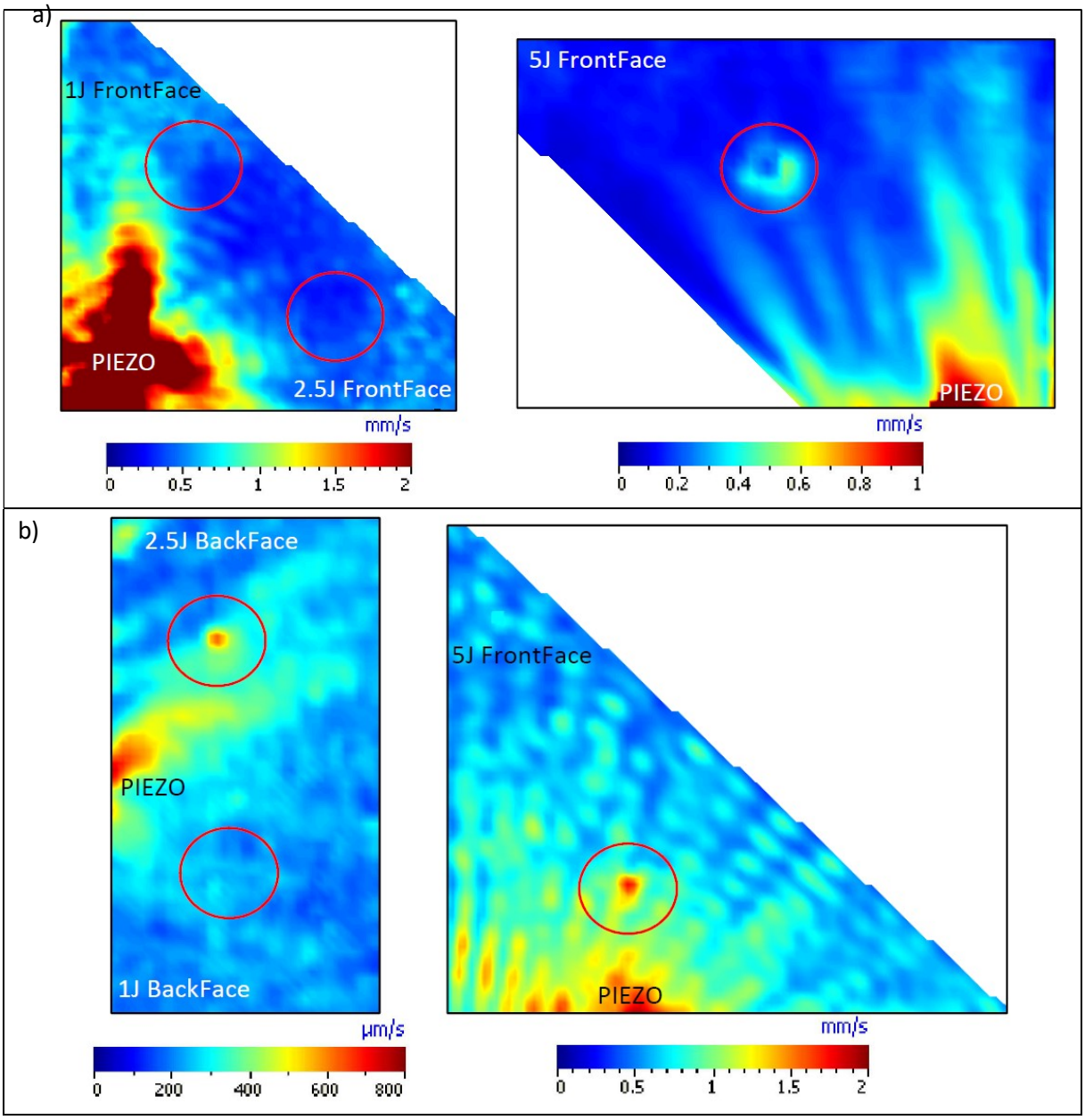

Figure 16. RMS values for a) HE1 samples, b) GE1 samples (frequency of excitation: 100 kHz, voltage: 200Vpp).

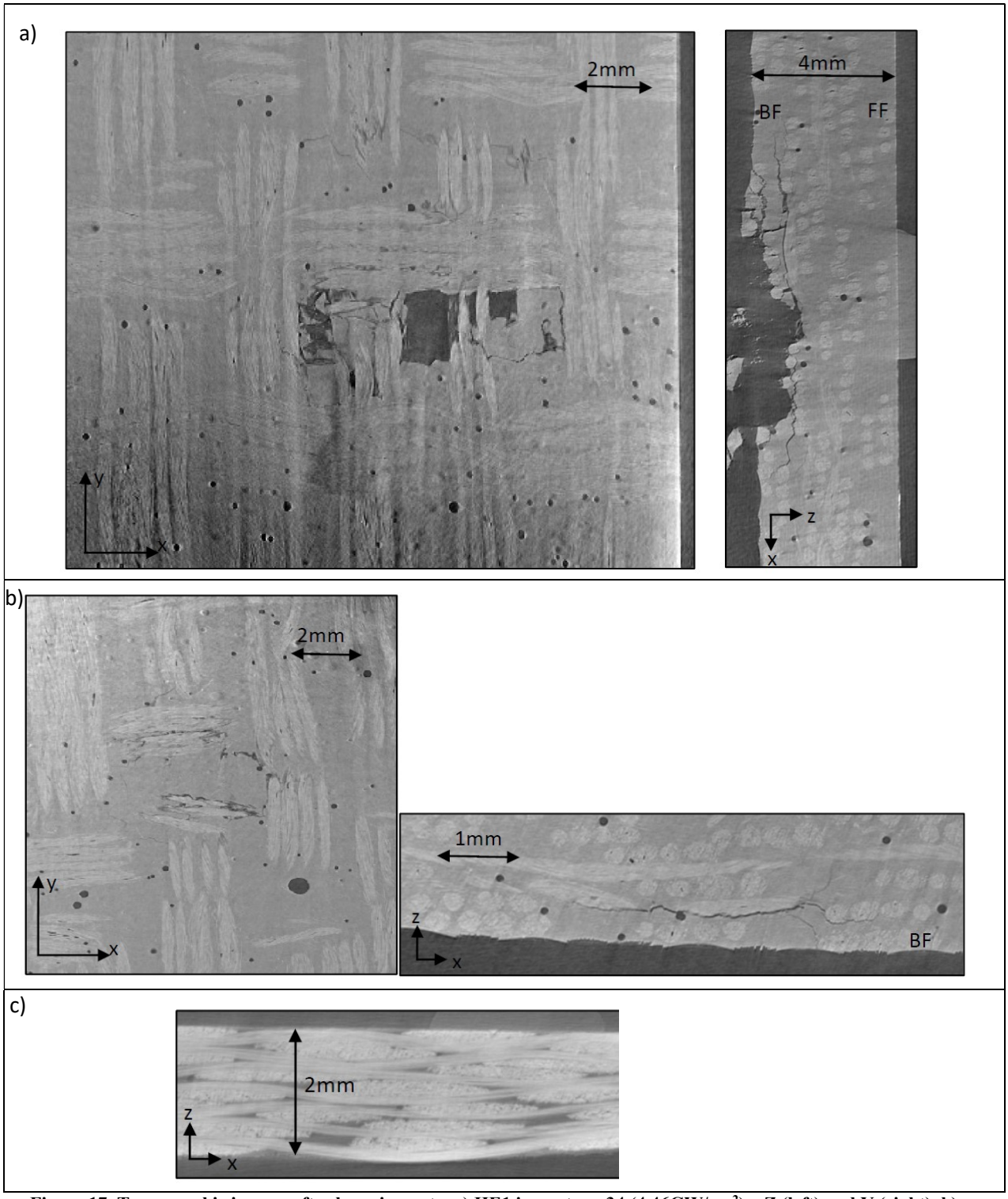

Figure 17. Tomographic images after laser impacts: a) HE1 impact no. 34 (4.46GW/cm^2) – Z (left) and Y (right), b) HE1 impact no. 35 (2.24GW/cm^2) – Z (left) and Y (right), c) GE1 impact no. 22 (4.55GW/cm2) –Y direction.

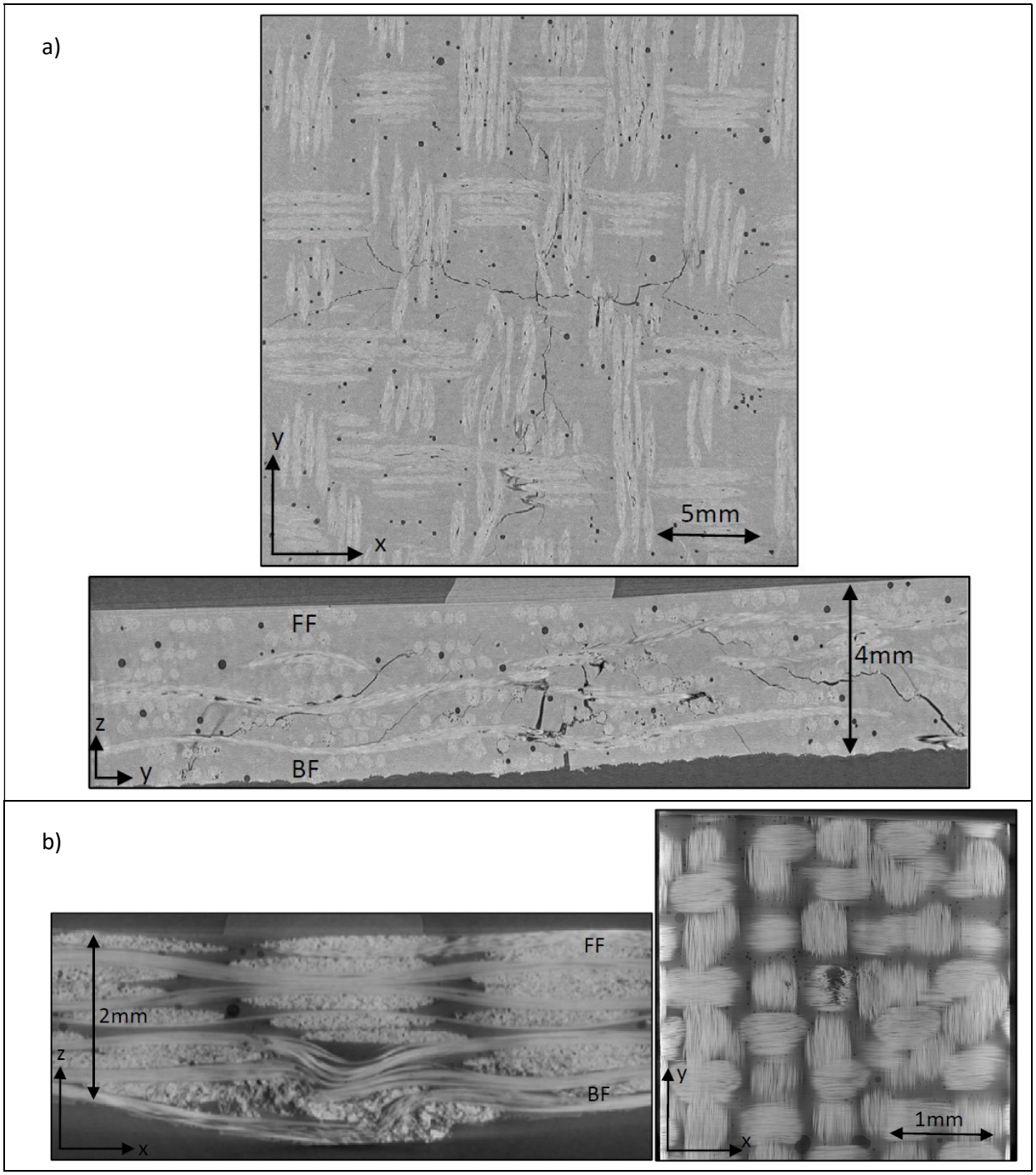

Figure 18. Tomographic images of mechanically impacted samples at 2.5J: a) HE1 images: Z (top), X (bottom), b) GE1 images: Y (left), Z (right).

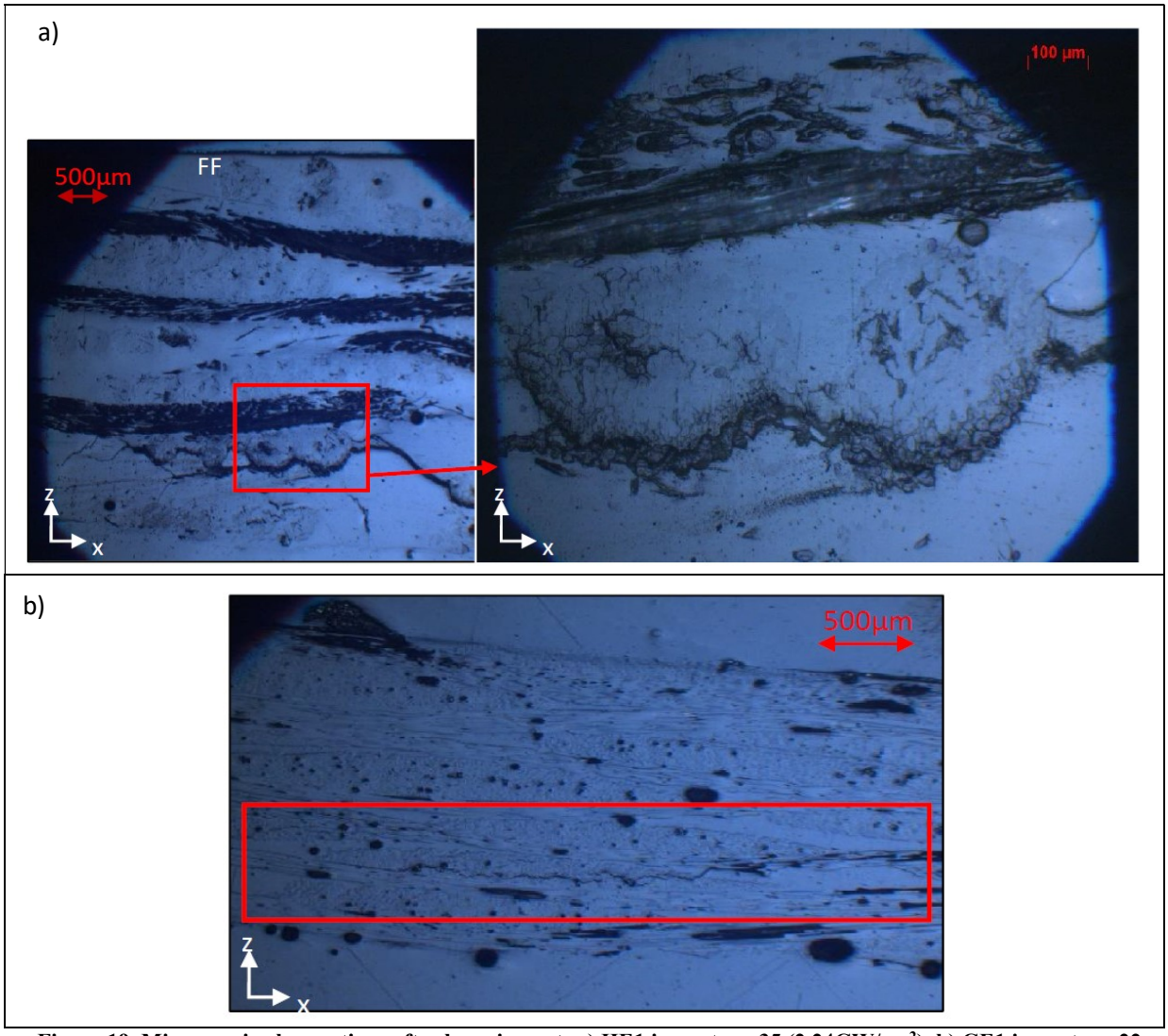

Figure 19. Microscopic observations after laser impact: a) HE1 impact no. 35 (2.24GW/cm^2), b) GE1 impact no. 22 (4.55GW/cm2).

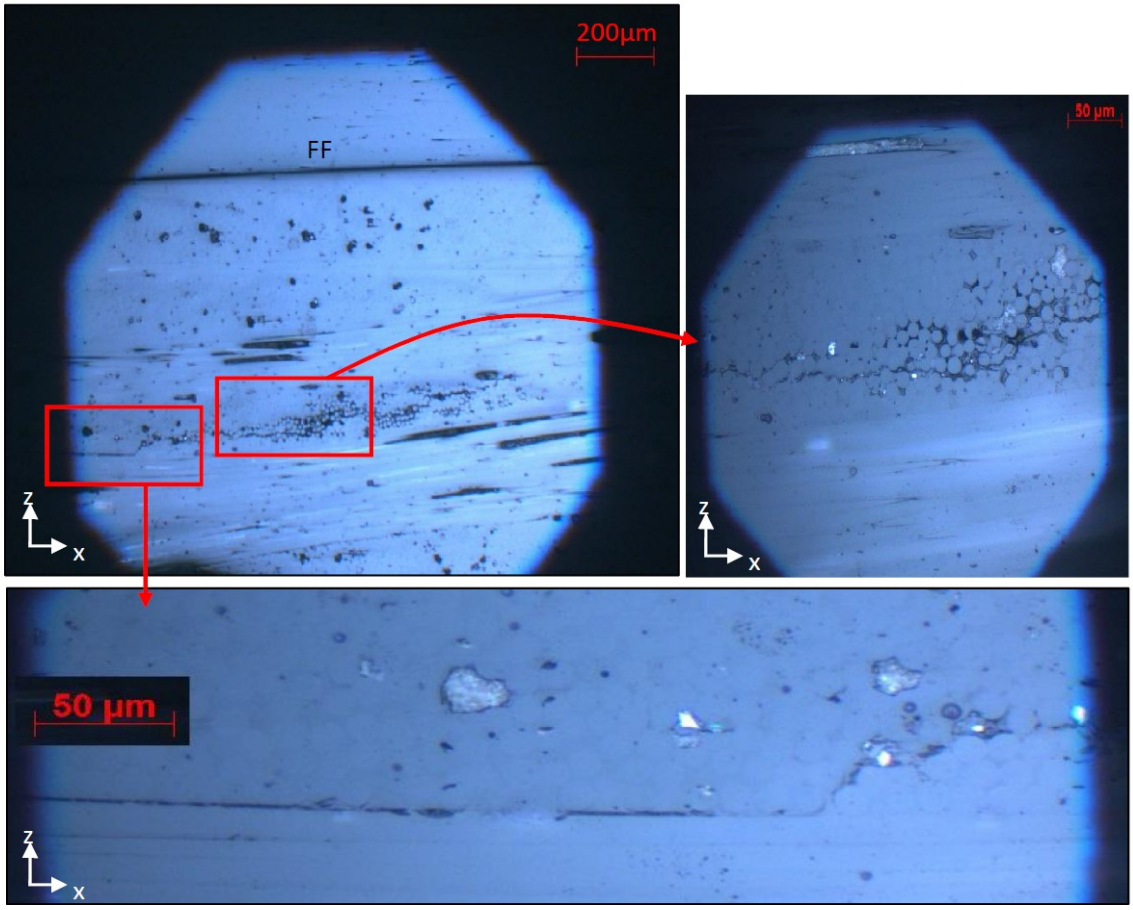

Figure 20. Mechanically impacted GE1 sample at 1J – microscopic observations

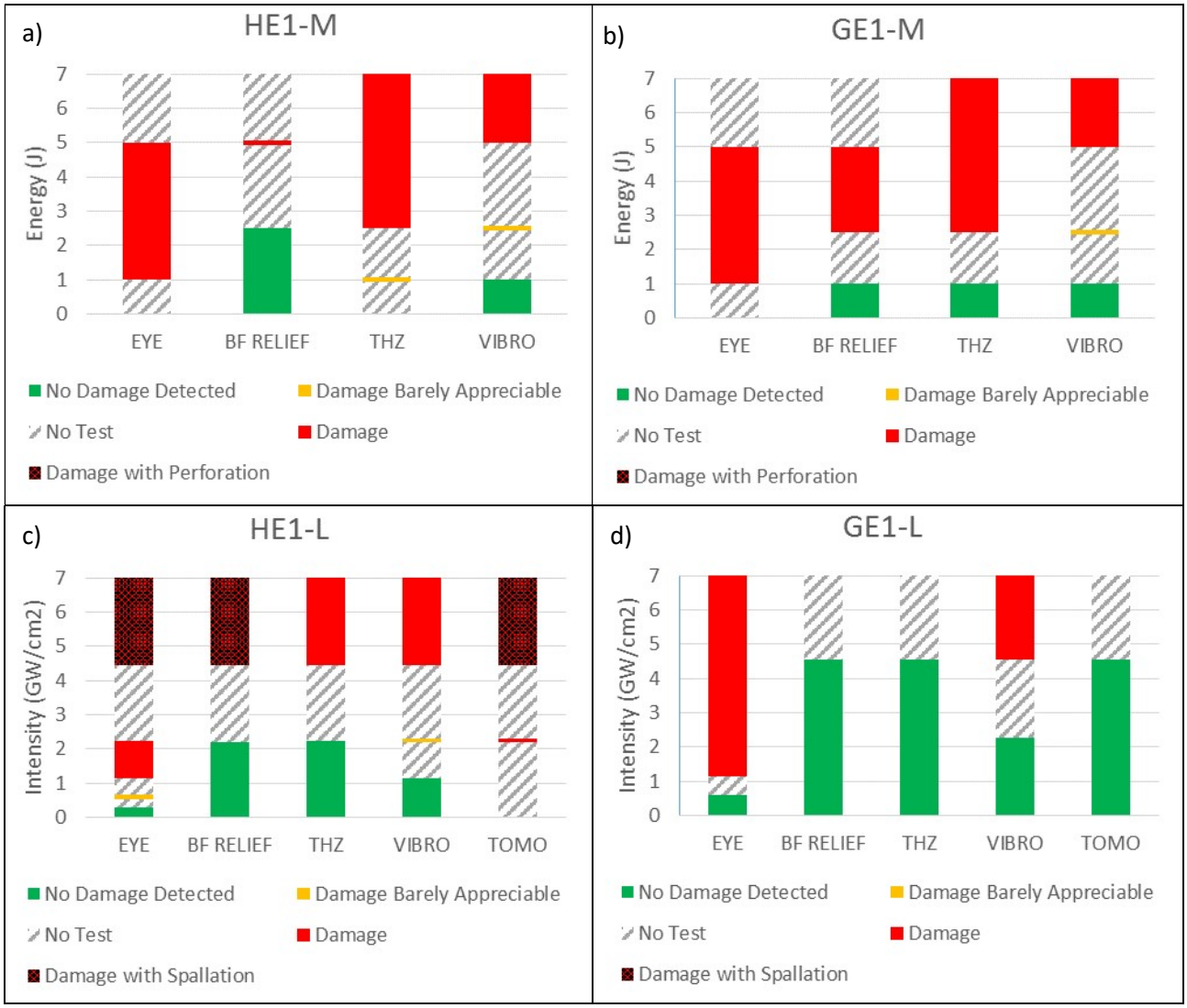

Figure 21. Damage detection thresholds for HE1 and GE1 samples: a) and b) after mechanical impacts, c) and d) after laser impacts.

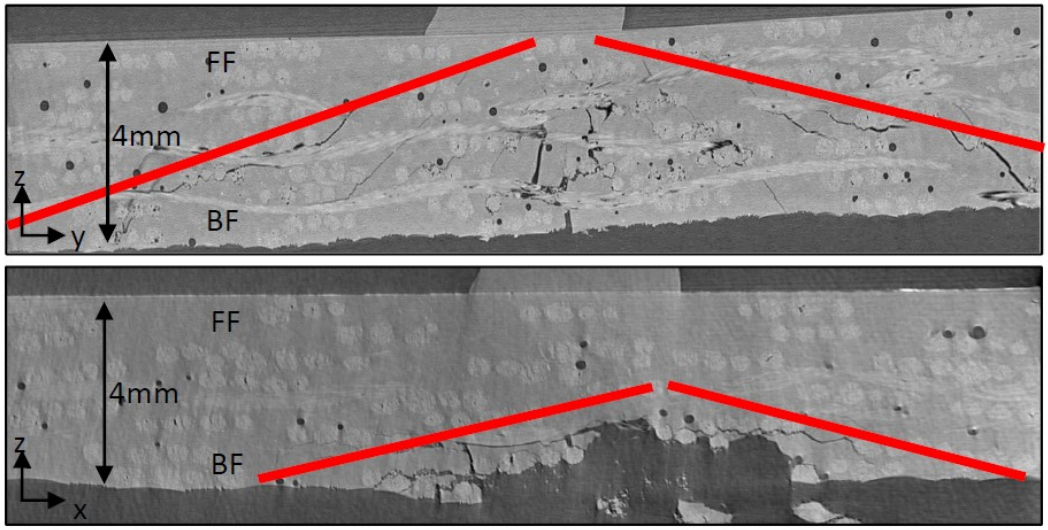

Figure 22. Tomographic images: X of HE1 at 2.5J (up) and Y of HE1 at 4.46GW/cm2 (no. 34) (down).